LA-UR-18-29629
Approved for public release; distribution is unlimited.

Title: Milestone Report: Grain growth and fission gas behaviour in doped UO2
M2MS-18LA0201034

Author(s): Cooper, Michael William Donald
Greenquist, I
Tonk, MR
Pastore, G
Shirvan, K
Stanek, Christopher Richard
Andersson, Anders David Ragnar

Intended for: Report

Issued: 2018-10-10

Milestone Report: Grain growth and fission gas behaviour in doped UO_2

M2MS-18LA0201034

M. W. D. Cooper[a], I. Greenquist[b], M. R. Tonks[b], G. Pastore[c], K. Shirvan[d], C. R. Stanek[a], D. A. Andersson[a]

[a]*Materials Science and Technology Division, Los Alamos National Laboratory P.O. Box 1663, Los Alamos, NM 87545, USA*
[b]*Department of Materials Science and Engineering, University of Florida, 158*
[c]*Fuel Modeling and Simulation Department, Idaho National Laboratory P.O. Box 1625, Idaho Falls, ID 83415, USA*
[d]*Department of Nuclear Science and Engineering, Massachusetts Institute of Technology, 77 Massachusetts Avenue, Cambridge, 02114 MA, USA*

Abstract

The microstructure of UO_2 can be modified during nuclear fuel fabrication by using additives. Several dopants (e.g. Cr, Ti, V, Mg, Nb) are used to enhance grain growth and densification during sintering. In previous work, we used atomic scale simulation techniques to identify a common interstitial solution mechanism for a range of dopants that form positively charged defects at sintering temperatures. As a result, negatively/positively charged defect concentrations were enhanced/supressed relative to undoped fuel under the same conditions (temperature and oxygen partial pressure). Importantly U and fission gas migration is vacancy mediated, such that the increase in the concentration uranium vacancies (which have negative charge), due to doping, causes an increase in U and fission gas diffusivity. This is important because U diffusivity is the rate limiting step in mass transport during sintering and bulk fission gas diffusivity is the underlying property that governs fission gas release. In this work, we implement analytical expressions for uranium vacancy concentrations in doped fuel (based on atomic scale results) into mesoscale and engineering scale simulations of sintering and fission gas release. It is shown that densification is dramatically enhanced at 1850 K and 1950 K due to dopant solution and that Mn-doping has a greater effect than the more widely used Cr-doping. The effect of both dopants is strongly temperature dependent and is negligible below approximately 1800 K. The effect of enlarged grain size and enhanced fission gas diffusivity has been included in BISON. Fuel temperatures under normal operating conditions are not sufficient to activate the enhanced fission gas diffusivity mechanism predicted by atomic scale calculations. Therefore, the benefits of enlarged grains for reduced fission gas release should not undermined by enhanced fission gas diffusivity for doped UO_2.

Email address: cooper_m@lanl.gov (M. W. D. Cooper)

1. Introduction

Conventional nuclear fuel for light water reactors (LWRs) consists of UO_2 fuel pellets encased in zircalloy rods. Although other materials have been or are being considered, UO_2 remains the dominant fuel pellet material due to its radiation tolerance, chemical stability, and high melting point (which offsets its poor thermal conductivity). During reactor operation, U fissions into many isotopes from across the periodic table. The fission gases, Xe and Kr, are produced in relatively large quantities and form inter- and intra-granular bubbles due to vanishingly low solubility in the host UO_2 lattice [1]. The growth and percolation of inter-granular bubbles eventually leads to venting of fission gas into the fuel plenum. This causes a reduction of the fuel-clad gap thermal conductivity, further fission gas release (FGR), and eventual rod failure due to over pressurization. Initially created as energetic fission fragments, the fission gas comes to rest in the UO_2 lattice. The diffusivity of fission gas in bulk UO_2 is the underlying property that governs the rate of FGR. Consequently, the promotion of enlarged grains during fuel fabrication is considered beneficial to reduced FGR as it extends the rate limiting intra-granular diffusion step. A range of dopants, Cr [2–7], Nb [8–10], Mg [10–12], Ti [10, 13], and V [14], have been identified experimentally as UO_2 grain enlargers for pellet fabrication. Increased plasticity is advocated as an additional benefit of enlarged grains [15].

Cr-doped UO_2 is the most widely studied doped fuel concept and has been adopted by several fuel vendors. Liquid phase sintering, associated with the CrO eutectic, is frequently touted in the literature as the mechanism for enhanced grain size [2–6]. However, the experimental study by Bourgeois et al. [2] shows two peaks in grain size as a function of dopant content. The peak at the solubility limit for Cr in UO_2 indicates a solid solution mechanism and the second peak well in excess of the solubility limit indicates a liquid phase sintering mechanism. This is further supported given the former peak persists even below the CrO eutectic temperature, whereas the latter does not. Our recent atomic scale simulations [16, 17] have revealed a common interstitial-type solution mechanism for several dopants (Cr, Mn, Fe, Mg, V, and Ti) under sintering conditions (above 1750 K). The common feature of such dopants is a chemistry that enables them to access either 1+ or 2+ charge states when occupying the interstitial site. For Cr, Mn, Fe, V, and Ti this is enabled by the ability of transition metals to occupy many different charge states with similar energies. For Mg, 2+ is its nominal charge state. Conversely, Al which has a strict 3+ charge state was found have interstitial concentrations orders of magnitude lower than the other dopants.

In our previous milestone [16] and paper [17] on the atomistic results, we discuss how the high interstitial concentrations (exhibited by Cr, Mn, Fe, Mg, V, and Ti) introduces extrinsic positive charge to the system that enhances the concentrations of the negatively charged uranium vacancies. The uranium vacancy concentration is coupled proportionally to the diffusivity of uranium and fission gas, which exhibit vacancy-mediated migration mechanisms [18]. Assuming an ideal grain growth mechanism that is diffusion controlled, Figure 1 [17] shows the doped UO_2 uranium vacancy concentrations as function of temperature (with undoped UO_2 included as a reference) alongside the estimated enhancement in grain size due each dopant.

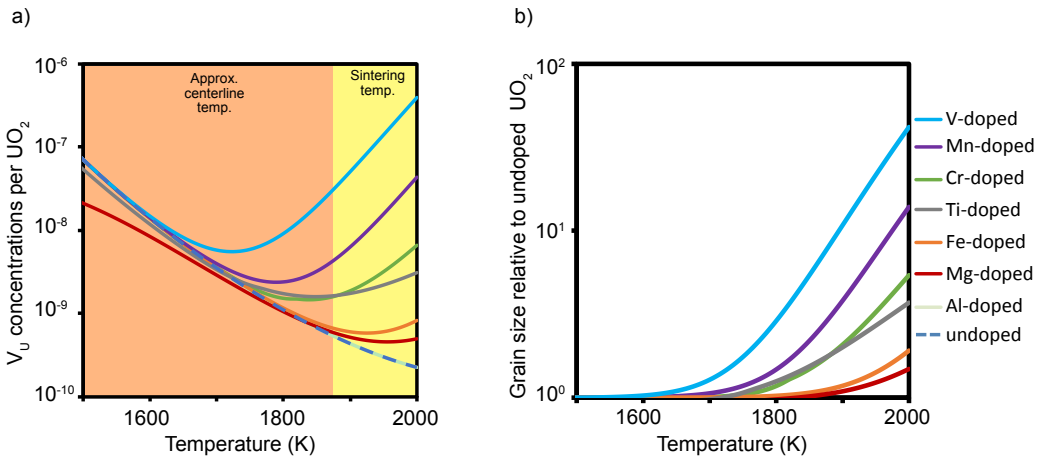

Figure 1: a) Comparison of the V_U concentrations in undoped and (Mg/Al/Ti/V/Cr/Mn/Fe)-doped UO_2 at temperatures relevant to the fuel centerline and for sintering with an O partial pressure of 10^{-20} (atm). b) The grain size enhancement with respect to undoped UO_2 assuming diffusion dominated ideal grain growth. Taken from Ref. [17].

In this report, we present an update on efforts to couple the atomistic results shown in Figure 1a to longer length and time scale simulations of sintering and FGR. Firstly, the analytical forms and physics that capture the effect of doping on U and fission gas diffusivity are discussed. Secondly, the results of phase field simulations of sintering are shown, including a comparison of Mn and Cr doping. Thirdly, results on FGR using BISON are presented. The underlying models that describe U and fission gas diffusivity based on atomic scale simulations were developed at LANL, the work on phase field simulations was carried out by M Tonks and I Greenquist at the University of Florida (funded by NEAMS through INL), and the fuel performance simulations were carried by G Pastore at INL and K Shirvan at MIT.

2. Methodology

2.1. Atomic scale calculations

The defect concentrations used in this work were calculated in previous reports and papers [16, 17]. Details of the DFT and empirical potential methodologies used can be found in Ref. [17]. Figure 1a shows the prediced uranium vacancy concentrations at the temperatures where the dopants have significant effect. Below this temperature (with the exception of Mg) the doped-UO_2 concentrations were identical to undoped UO_2 due to low dopant solubility.

2.2. Phase field simulations

2.2.1. The existing phase field model

The description of the phase field simulations that follows is provided to give context to the implementation of the atomic scale simulation results. The information below is taken from

a progress report by Greenquist and Tonks [19]. The microstructural evolution of undoped and doped UO_2 has been simulated using the Grand Potential Model [20, 21] implemented within the MARMOT [22] phase field code. The solid phase is represented by a set of non-conserved order parameters, $\vec{\eta} = \eta_1, \eta_2, ..., \eta_n$ that represent the various grains. These variables are governed by the Allen-Cahn equation:

$$\frac{\partial \eta_i}{\partial t} = -L_s \frac{\delta \Omega}{\delta \eta_i} \tag{1}$$

where L_s is the solid phase mobility and Ω is the grand potential function. The void phase is also represented by a non-conserved order parameter, ϕ. This is also represented by the Allen-Cahn equation

$$\frac{\partial \phi}{\partial t} = -L_v \frac{\delta \Omega}{\delta \phi} \tag{2}$$

where L_v is the void phase mobility.

The conserved variable representing the uranium vacancy concentration is defined as c. However, c is not solved directly, but is instead a function of the chemical potential, μ, which is governed by the potential evolution equation:

$$\frac{\partial \mu}{\partial t} = \frac{1}{\chi}\left[\nabla \cdot (\chi \mathbf{D} \nabla \mu) - \frac{1}{V_a} \sum_i \frac{\partial c}{\partial \eta_i} \frac{\partial \eta_i}{\partial t}\right] \tag{3}$$

where χ is the susceptibility, $\mathbf{D}$ is the diffusivity tensor [23], and V_a is the atomic volume of Uranium.

The grand potential function, Ω, is defined in Ref. [21] where it is modified from the free energy function in Ref. [24]:

$$\Omega = \int_V \left(\epsilon \left[\left(\frac{\phi^4}{4} - \frac{\phi^2}{2} \right) + \sum_i \left(\frac{\eta_i^4}{4} - \frac{\eta_i^2}{2} \right) + \gamma \left(\phi^2 \sum_i \eta_i^2 + \sum_i \sum_{j>i} \eta_i^2 \eta_j^2 \right) + \frac{1}{4} \right] + \frac{\kappa}{2} \left[(\nabla \phi)^2 + \sum_i (\nabla \eta_i)^2 \right] + h_s \omega_s + h_v \omega_v \right) dV. \tag{4}$$

In Eq. (4), ϵ is a function defining the surface and grain boundary (GB) energies, κ is a function that determines the gradient energy, which controls interface widths. $\gamma = 1.5$ controls the interface symmetry. h_s and h_v are switching functions that determine the phase subject to the constraint $h_s + h_v = 1$, and ω_s and ω_v are the local potential densities of each phase.

The local potentials (ω_β, $\beta = s, v$) are derived from the local free energies f_β. f_v is an unphysical quantity because there is no energy associated with the void. However, it is required for the model with the requirement that it has a minimum at $c = 1$. Therefore, a simple quadratic free energy is defined:

$$f_v = \frac{1}{2} k_v (c - 1)^2 \tag{5}$$

where k_v is a parabolic constant that defines the slope of the energy function.

In the solid phase, however, the energy function follows the ideal solution model:

$$f_s = f_A(T) + \frac{cE_f}{V_a} + \frac{k_B T}{V_a}\left[c\ln(c) + (1-c)\ln(1-c)\right], \tag{6}$$

where $f_A(T)$ is an adjustment function that keeps the minima of the two phase energies equal, E_f is the vacancy formation energy, T is the absolute temperature, and k_B is the Boltzmann constant.

For more information about converting between c and μ and between f_β and ω_β, see Ref. [20]. Following the conversion processes described in Ref. [20], the solid-phase vacancy concentration can be calculated as

$$c(\mu) = \frac{\exp\left(\frac{\mu - E_f}{k_B T}\right)}{1 + \exp\left(\frac{\mu - E_f}{k_B T}\right)}, \tag{7}$$

and the equilibrium concentration is $c(\mu = 0)$.

2.2.2. Modifications based on atomic scale simulations

In order to simulated the impact that a dopant in solution can have on sintering it is necessary to couple the phase field model, described above, to predictions from atomic scale simulations. This is achieved in Section 3.1 by defining expressions for the equilibrium concentrations of uranium vacancies in undoped, Cr-doped and Mn-doped UO_2 based on on the predictions shown in Figure 1a. The expressions for bulk equilibrium vacancy concentrations are given in Equations (12) to (14) and the modification due to segregation that gives the grain boundary concentrations is described by Equation (15).

2.3. Fission gas release simulations

The simulation of FGR from a fuel pin was carried out in the BISON fuel perfomance code [25]. A more detailed description of the method can be found in the work of Che et al. [26], here we focus on the modifications made to couple those simulations to the atomic scale results [17]. In BISON the diffusion of fission gas within the grain to the grain boundaries is described in 1D spherical geometry by:

$$\frac{\partial C_t}{\partial t} = D_{eff}\frac{1}{r^2}\frac{\partial}{\partial r}\left(r^2\frac{\partial C_t}{\partial r}\right) + \beta \tag{8}$$

where C_t is the intra-granular fission gas concentration, β is the fission gas generation rate, r is the radial coordinate, t is time, and D_{eff} is the effective (perturbed) fission gas diffusivity [27]:

$$D_{eff} = D\frac{Fb_0}{Fb_0 + g} \tag{9}$$

where Fb_0 is the resolution rate (proportional to the fission rate F), and g is the trapping rate. D_{eff} is proportional to the unperturbed fission gas diffusivity, D, which is proportional to the concentration of the migration-mediating uranium vacancies.

The effect of doping can be considered two-fold: i) the increase in grain size is captured by Equation (8) and ii) changes to the fission gas diffusivity are described by scaling Equation (9), such that $D_{doped} = \frac{[V_U]_{doped}}{[V_U]_{undoped}} D_{undoped}$ where $\frac{[V_U]_{doped}}{[V_U]_{undoped}}$ is given by Equation (10) for Cr-doped UO_2.

3. Results and Discussion

3.1. Analytical expressions of vacancy concentrations

There are three distinct temperature regimes for the predicted defect concentrations that can be defined in terms of the dominant charge compensating defects in the system:

1. At low temperatures the system is dominated by the equilibrium of uranium vacancies and holes, $[\mathrm{V}_\mathrm{U}^{''''}] = 4[\mathrm{U}_\mathrm{U}^{\bullet}]$
2. At intermediate temperatures the system is dominated by the equilibrium of holes and electrons $[\mathrm{U}_\mathrm{U}^{\bullet}] = [\mathrm{U}_\mathrm{U}^{\prime}]$
3. At high temperatures the system is dominated by the equilibrium of the interstitial dopants and electrons $[\mathrm{X}_\mathrm{i}^{\bullet}] = [\mathrm{U}_\mathrm{U}^{\prime}]$ (where X is Cr or Mn in this study)

All other defects in the system are charge compensated by very small deviations in these relationships and within each region the formation energy of a given defect is fixed (such that Arrhenius functions can be fitted). Note that the effect of doping on the system is only seen when the dopant becomes one of the dominant charge compensating defects and, as such, modifies the formation energy of the other defects (e.g. uranium vacancies) [17]. The transition to the high temperature regime is governed by sufficiently high dopant solubility that it becomes a dominant charge compensating defect, thus, modifying the Fermi-level through $[\mathrm{U}_\mathrm{U}^{\bullet}] = [\mathrm{U}_\mathrm{U}^{\prime}] \rightarrow [\mathrm{X}_\mathrm{i}^{\bullet}] = [\mathrm{U}_\mathrm{U}^{\prime}]$.

The enhancement of uranium vacancy concentrations due to doping can be captured by the fraction $\frac{[\mathrm{V}_\mathrm{U}^{''''}]_{doped}}{[\mathrm{V}_\mathrm{U}^{''''}]_{undoped}}$. The Cr-doped and Mn-doped UO_2 uranium vacancy concentrations normalised against the undoped case are given by:

$$\frac{\left[\mathrm{V}_\mathrm{U}^{''''}\right]_{Cr-doped}}{\left[\mathrm{V}_\mathrm{U}^{''''}\right]_{undoped}} = \begin{cases} 1.0, & \text{for } 300\ K < T < 1833\ K, \\ 8.78 \times 10^{19} \exp\left(\frac{-7.134\ \mathrm{eV}}{k_B T}\right), & \text{for } 1833\ K < T < 2000\ K \end{cases} \tag{10}$$

$$\frac{\left[\mathrm{V}_\mathrm{U}^{''''}\right]_{Mn-doped}}{\left[\mathrm{V}_\mathrm{U}^{''''}\right]_{undoped}} = \begin{cases} 1.0, & \text{for } 300\ K < T < 1833\ K, \\ 4.65 \times 10^{21} \exp\left(\frac{-7.143\ \mathrm{eV}}{k_B T}\right), & \text{for } 1776\ K < T < 2000\ K \end{cases} \tag{11}$$

where $[\mathrm{V}_\mathrm{U}^{''''}]_{Cr-doped}$, $[\mathrm{V}_\mathrm{U}^{''''}]_{Mn-doped}$, and $[\mathrm{V}_\mathrm{U}^{''''}]_{undoped}$ are the uranium vacancy concentrations in Cr-doped, Mn-doped, and undoped UO_2, respectively. k_B is the Boltzmann constant. Note that there are now only two regimes, given that both the low (1) and intermediate (2) temperature regimes are unaffected by doping (i.e. $\frac{[\mathrm{V}_\mathrm{U}^{''''}]_{doped}}{[\mathrm{V}_\mathrm{U}^{''''}]_{undoped}} = 1.0$ for both). Due to the proportionality

between fission gas diffusivity and the uranium vacancy concentration, Equation (10) is used to scale the (undoped) fission gas diffusivity used in Equations (8) and (9) to enable BISON simulations of FGR from Cr-doped UO_2.

The enhanced uranium vacancy concentrations were determined [17] using the Busker potential [28] for the calculation of the vibrational entropy of defects because, unlike the CRG potential [29], it includes parameters for the dopants. The undoped UO_2 concentrations were also calculated using the CRG potential for vibrational entropy, which provides a better description of the host UO_2 lattice and predicts higher uranium vacancy concentrations than the Busker potential [28–30]. To achieve the benefits of both potentials, $\frac{[V_U'''']_{Cr-doped}}{[V_U'''']_{undoped}}$ and $\frac{[V_U'''']_{Mn-doped}}{[V_U'''']_{undoped}}$ have been combined with $[V_U'''']_{undoped}$ from the CRG the potential, giving:

$$\left[V_U''''\right]_{undoped} = \begin{cases} 1.1185\times10^{-4}\exp\left(\frac{0.2134\text{ eV}}{k_BT}\right), & \text{for } 1000\ K < T < 1263\ K, \\ 1.1772\times10^{-15}\exp\left(\frac{2.971\text{ eV}}{k_BT}\right), & \text{for } 1263\ K < T < 2000\ K \end{cases} \tag{12}$$

$$\left[V_U''''\right]_{Cr-doped} = \begin{cases} 1.1185\times10^{-4}\exp\left(\frac{0.2134\text{ eV}}{k_BT}\right), & \text{for } 1000\ K < T < 1263\ K, \\ 1.1772\times10^{-15}\exp\left(\frac{2.971\text{ eV}}{k_BT}\right), & \text{for } 1263\ K < T < 1803\ K, \\ 1.0334\times10^{5}\exp\left(\frac{-4.163\text{ eV}}{k_BT}\right), & \text{for } 1803\ K < T < 2000\ K \end{cases} \tag{13}$$

$$\left[V_U''''\right]_{Mn-doped} = \begin{cases} 1.1185\times10^{-4}\exp\left(\frac{0.2134\text{ eV}}{k_BT}\right), & \text{for } 1000\ K < T < 1263\ K, \\ 1.1772\times10^{-15}\exp\left(\frac{2.971\text{ eV}}{k_BT}\right), & \text{for } 1263\ K < T < 1772\ K, \\ 5.480\times10^{6}\exp\left(\frac{-4.1625\text{ eV}}{k_BT}\right), & \text{for } 1772\ K < T < 2000\ K \end{cases} \tag{14}$$

where these functions represent the absolute bulk vacancy concentrations in undoped and doped UO_2. In the phase field simulations of sintering Equations (12) to (14) are used to defined the equilibrium concentration of defects in bulk UO_2 (i.e. solid phase fraction = 1).

The bulk uranium vacancies experience a decreasing potential energy surface as they move towards the grain boundary, see schematic in Figure 2. Hence, the concentration of vacancies in the grain boundary is in equilibrium with with the vacancy concentration in the bulk. This equilibrium can be described it its simplest form by using a single segregation energy, as such:

$$[v_U'''']_{GB} = [v_U'''']_{Bulk}\exp\frac{-E_{seg}}{k_BT} \tag{15}$$

where $[v_U'''']_{GB}$ and $[v_U'''']_{bulk}$ are the grain boundary and bulk vacancy concentrations, respectively. E_{seg} is the segregation energy. Figure 3 shows $[v_U'''']_{Bulk}$ (black lines) and $[v_U'''']_{GB}$ (colored lines) for undoped UO_2 (solid lines) and Cr-doped UO_2 (dashed lines). The use of Equation (15) assumes that the vibrational entropy of a uranium vacancy is unchanged due to segregation and that the following effects can be captured by a single effective E_{seg}: i) variations in E_{seg} between grain boundary types, ii) different E_{seg} for various vacancy sites within a single grain boundary, and iii) the vacancy-vacancy interactions for non-dilute defect concentrations. The validity of these assumptions will be explored later.

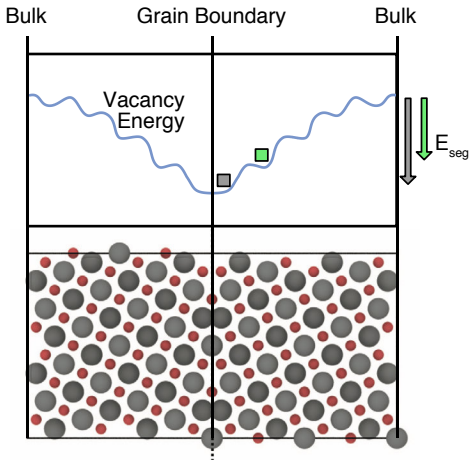

Figure 2: A $\Sigma 5$-tilt grain boundary with a schematic of the energy landscape (blue line) experienced by a uranium vacancy as a function of distance from the grain boundary. The grey and green squares indicate the lowest and second lowest energy sites for a vacancy, respectively.

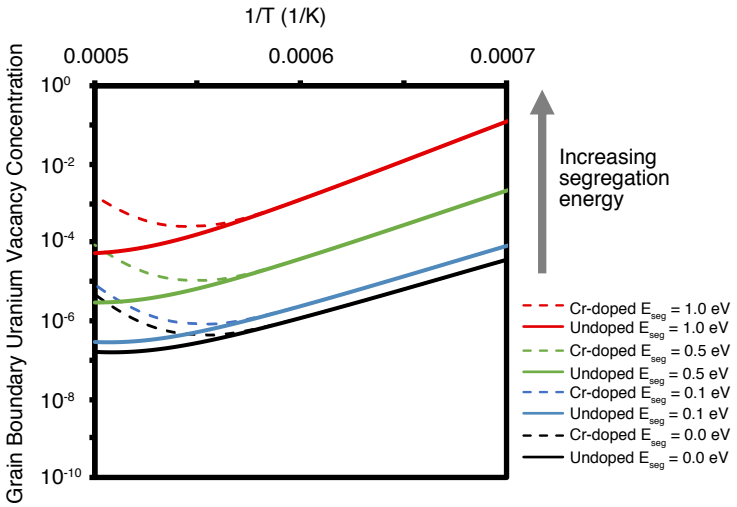

Figure 3: The grain boundary concentrations of undoped (solid lines) UO_2 and Cr-doped (dashed lines) UO_2 using Equation (15) with several values of E_{seg}. Bulk values are given by $E_{seg} = 0$.

3.2. Phase field simulations - sintering

All phase field simulations were carried out using the same 2D mesh of 2000×2000 nm, representing four circular particles of 400 nm in a square arrangement, see Figure 4. Although a 3D mesh might be more representative of sintering, the 2D model is suitable for the purposes of this study, which focuses on exploring the coupling of atomic scale calculations to phase field simulations.

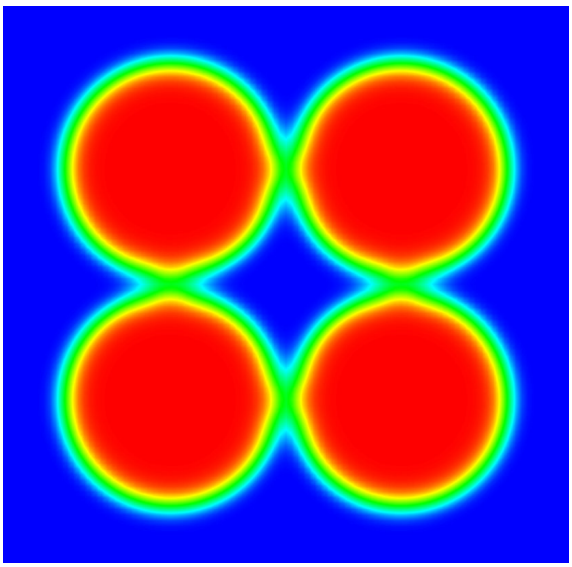

Figure 4: The initial conditions of a four particle sintering simulation. Red represents a solid fraction of 1 and blue represents a solid fraction of 0 (i.e. a void), whereby other colors indicate the interfaces.

The pore structure shown in Figure 4 was evolved for undoped, Cr-doped, and Mn-doped UO_2 at 1750 K, 1850 K and 1950 K until the final condition (pore closure) was attained, see Figure 5. During the simulations mass is transported, either by bulk or grain boundary diffusion, to the central void, thus, minimising the solid-void interfaces by closing the pore and reducing the energy of the system.

Figure 6 shows the surface area of the central void as a function of time for undoped and Cr-doped UO_2, with the bulk vacancy concentration modified according to doping, but the grain boundary vacancy concentration fixed at 0.1 for both doped and undoped UO_2. The results show that modifying the bulk concentrations has no effect on pore closure rates. Therefore, it is clear that in this case the dominant pathway for migration of vacancies from the central pore to the exterior of the system is along the grain boundaries.

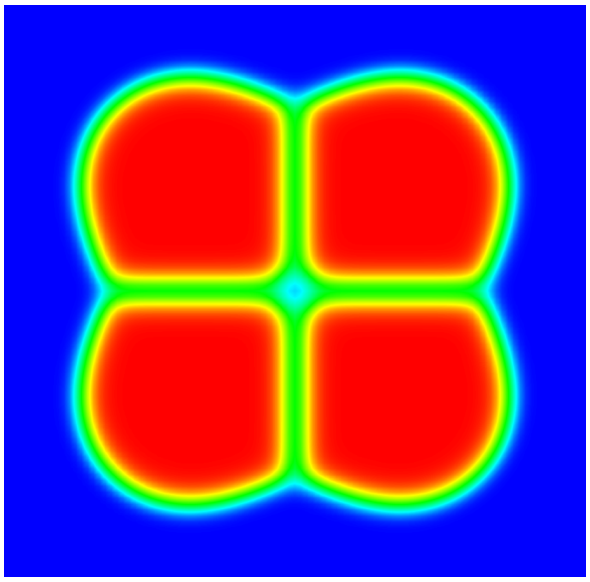

Figure 5: The final conditions of a four particle sintering simulation, showing pore closure. Red represents a solid fraction of 1 and blue represents a solid fraction of 0 (i.e. a void), whereby other colors indicate the interfaces.

The energy of a vacancy decreases as it is moved from the bulk to the grain boundary. Therefore, the grain boundary concentrations should be described as in equilibrium with the bulk concentration via the difference in the uranium vacancy energy from the bulk to grain boundary (E_{seg}), as shown in Equation (15) and Figure 3. The four-particle sintering simulation was run again using an E_{seg} of 1.0 eV and 1.5 eV to couple the grain boundary vacancy concentrations to the bulk values, thus, capturing the effect of the dopant, see Figure 7. Firstly, note that the pore closure rate is significantly reduced compared to Figure 6 given the grain boundary concentrations are all well below 0.1, as used before. For both E_{seg} = 1.0 eV and 1.5 eV the Cr-doped UO_2 pore closure rate greatly exceeds that of undoped UO_2. Going forward E_{seg} = 1.5 eV is selected as it gives reasonable densification rates for undoped UO_2 (full densification in hours).

In our previous atomistic work, Mn was proposed as a more effective sintering aid than Cr. Figure 8 shows the pore size as a function of temperature for undoped, Cr-doped, and Mn-doped UO_2 for 1750 K, 1850 K, and 1950 K. The first observation that stands out is that the densification rate decreases as a function of temperature for undoped UO_2. This contradicts experimental observation of sintering rates [2] and indicates decreasing U diffusivity at the grain boundaries as a function of temperature (i.e. a negative activation energy). The activation

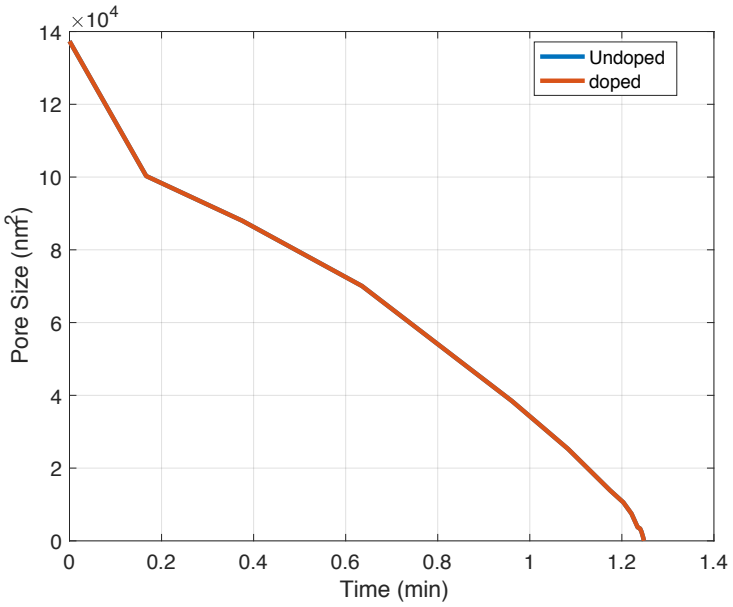

Figure 6: The pore size as a function of time. The simulations were carried out at 1950 K by using differenent bulk vacancy concentrations for undoped and Cr-doped but by keeping the grain boundary concentration fixed at 0.1.

energy for grain boundary diffusion is the sum of i) the bulk vacancy formation energy (E_f), ii) the segregation energy (E_{seg}), and iii) the migration barrier for uranium vacancies (E_{mig}, taken from experiment [31]). In our current model $E_f - E_{seg} + E_{mig} < 0$. For the formation energy and the segregation energy there are certain assumptions within the model that could explain the negative activation energy:

- The undoped formation energy used in our model is negative. This is shown by the decrease in uranium vacancy concentration associated with the reduction of UO_{2+x} to UO_2, as the oxygen potential decreases with temperature for a fixed oxygen partial pressure (see Figures 1 and 3). This ignores the buffering reactions that occur in real life (e.g. due to moisture in the furnace), which increase the oxygen partial pressure at higher temperatures. This limits the decrease in the oxygen potential and will result in a smaller decrease in the uranium vacancy concentration as function of temperature. It is possible that a more full treatment of oxygen partial pressure will reverse the trend of decreasing densification with increasing temperature for undoped UO_2 by making the uranium vacancy formation energy less negative.

- The description of segregation energy as a fixed value does not account for concentration dependence, which would effectively reduce the segregation energy for high grain boundary vacancy concentrations. There are three components of concentration depen-

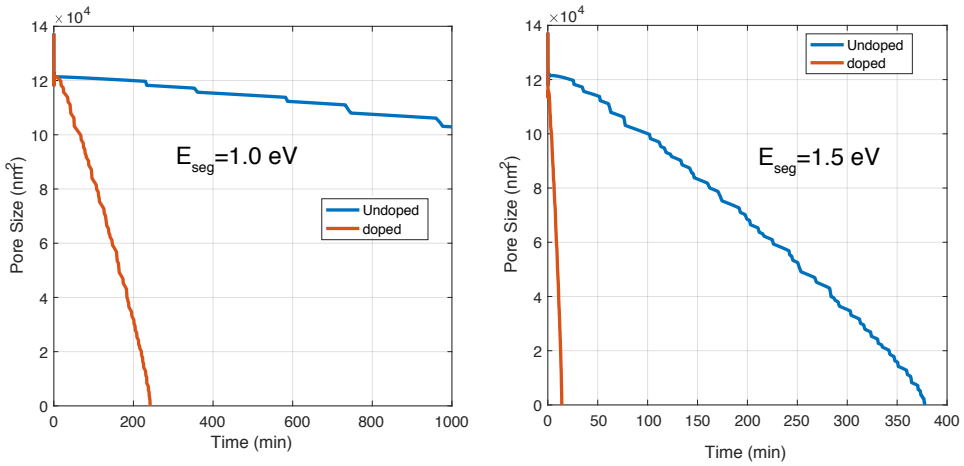

Figure 7: The pore size as a function of time. The simulations were carried out at 1950 K by using differenent bulk vacancy concentrations for undoped and Cr-doped. The grain boundary vacancy concentrations were coupled to the bulk by using E_{seg} of 1 eV or 1.5 eV.

dence to be considered. Firstly, more than one vacancy cannot occupy the same site at the same time, meaning that as the low energy sites become fully occupied further segregation is forced to occur via sites that exhibit weaker segregation (this is shown for the red vacancy in Figure 2). Secondly, if these sites are close to each other vacancy-vacancy interactions might be significant. Thirdly, given the ionic nature of UO_2, uranium vacancies carry with them negative charge. Therefore, the accumulation of space charge at the grain boundaries creates an electrostatic repulsion that reduces the segregation of additional vacancies. Both of these effects might be significant in reducing the segregation energy and reversing the temperature dependence of densification predicted for undoped UO_2.

Alternatively, it is possible that the assumption of a constant grain boundary energy is flawed. If the surface energy increases with temperature then this might counteract the negative activation energy for grain boundary diffusion by increasing the driving force for pore size reduction. While this discussion highlights some of the questions and challenges that must be addressed to develop more accurate models, the relative effect of dopants on sinterability can still be examined.

As can be seen in Figure 8, neither dopant has any impact on the densification rate at 1750 K because their effect on uranium vacancy concentrations is negligible unless $T > 1803$ K for Cr and $T > 1772$ K for Mn. At 1850 K and 1950 K, pore size reduction occurs at a much greater rate for Mn-doped UO_2 compared to Cr-doped UO_2 or undoped UO_2. It is also worth noting

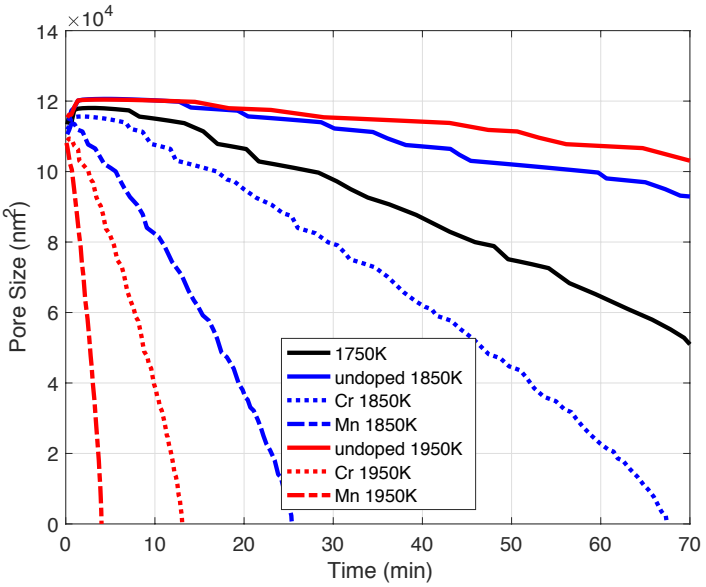

Figure 8: The pore size as a function of time. The simulations were carried out at 1750 K, 1850 K, 1950 K by using differenent bulk vacancy concentrations for undoped, Cr-doped, and Mn-doped. The grain boundary vacancy concentrations were coupled to the bulk by using an E_{seg} of 1.5 eV.

that for both doped UO_2 cases higher rates of pore closure occur for increasing temperature, reversing the trend seen for undoped UO_2. This is a result of the increase in uranium vacancy concentration seen as a function of temperature for both dopants (see Figures 1 and 3).

Further work should be done to improve coupling of the bulk UO_2 atomic scale simulations to the phase field models. In particular, a better understanding of the segregation of vacancies to grain boundaries would be beneficial. This will also be important as we develop grain boundary kinetics models that capture the effect of doping on both grain size and densification. Nonetheless, these simulations provide promise that Mn oxide could be a suitable sintering aid with potentially improved performance compared to Cr oxide.

3.3. *Fuel performance simulations - fission gas release*

Simulations were carried out using the BISON fuel performance code [25] to investigate the effect that doping has on FGR, via its impact of fission gas diffusivity. Previously, Che *et al.* [26] simulated Cr-doped UO_2 in BISON by scaling the fission gas diffusivity by a factor of 3 (based on experimental work carried out by Killeen at 1773 K [4]) and by using an average grain size of 55 μm. Fission gas exhibits a vacancy-mediated diffusion mechanism, whereby the diffusivity of fission gas scales proportionally to the equilibrium concentration of uranium vacancies. In this work, the same simulations as in Ref. [26] are repeated but instead the fission gas diffusivity is scaled by $\frac{[V_U]_{Cr-doped}}{[V_U]_{undoped}}$ from Section 3.1. The grain size of 55 μm was kept unchanged.

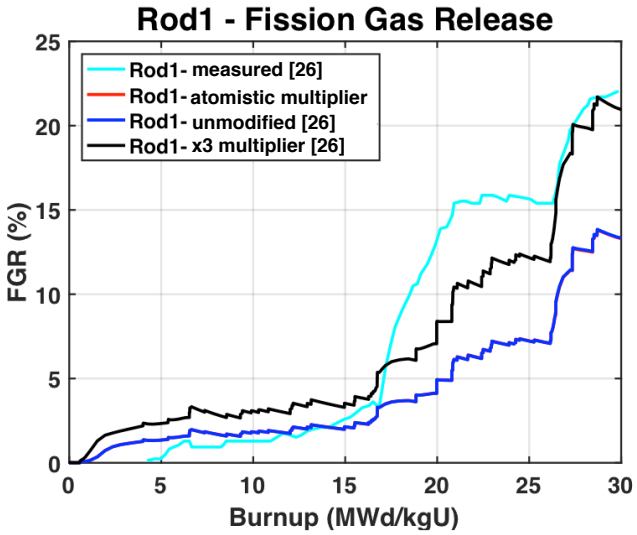

Figure 9: Fission gas release fraction as a function of burnup using fission gas diffusivity based on i) unmodified undoped UO_2 (dark blue line) [26], ii) a ×3 multiplier (black line) [26], and iii) the $\frac{[V_U]_{Cr-doped}}{[V_U]_{undoped}}$ multiplier from Section 3.1 (red line - hidden behind the unmodified data). A 55 μm grain size was used throughout. Comparison is made to data inferred from measurements of internal rod pressure during the Halden IFA-677.1 fuel rod experiment [26].

Figure 9 shows that implementation of a fission gas diffusivity model base on our atomic scale simulations has no impact whatsoever on FGR when compared to the unmodified (undoped) fission gas diffusivity model. Note that a 55 μm grain size was used in both cases and we are only discussing the impact of dopants on fission gas diffusivity in the context of FGR. This is an important result as it indicates that the benefits of large grains are not offset by higher

fission gas diffusivity associated with the dopant's effect on uranium vacancy concentrations. This can be understood given that the pellet operating temperatures in these simulations never exceed the threshold of 1803 K [26], below which our simulations predict $\frac{[V_U]_{Cr-doped}}{[V_U]_{undoped}} = 1$ and no impact on fission gas diffusivity.

The results of Che et al. [26] give a better comparison with the measured values. However, in order to achieve this result the ×3 multiplier has been applied over the entire temperature range. It is hard to infer that such a small change in the diffusivity is due to doping alone. For example, Turnbull *et al.* [32] show variations frequently of ×3 and even up to an order of magnitude between measurements of fission gas diffusivity in undoped UO_2. The uranium vacancy concentration (and fission gas diffusivity) is highly sensitive to deviations in oxygen partial pressure and is, thus, highly sensitive to small changes in the fabrication process. To emphasise that point, Figure 10 shows that a change in the oxygen partial pressure of just a factor of 3 results corresponds to a factor of 3 increase in the uranium vacancy concentration over a large temperature range and dominates the dopant effect for normal reactor operating temperatures (<1800 K).

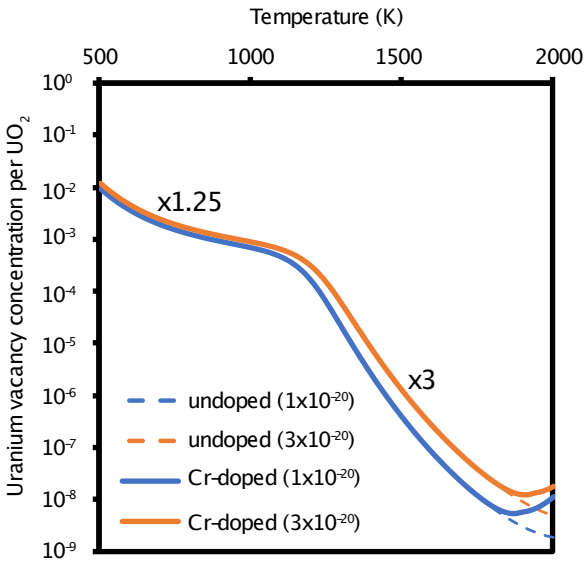

Figure 10: The uranium vacancy concentration using the atomic scale simulations method discussed in Ref. [17] for oxygen parital pressures of 1×10^{-20} and 3×10^{-20}.

4. Conclusions

UO_2 can be doped during fuel fabrication to increase grain size, promoting greater fission gas retention and higher plasticity. In previous work [16, 17], we provided insight into the mechanism for dopant solution in UO_2 and the change in host defect concentrations that arises due to doping. More specifically, the creation of interstitial dopant defects that are positively charged enhances the concentrations of negatively charged host defects (such as uranium vacancies). Fission gas and uranium diffusivities are mediated by uranium vacancies. In this work, analytical expressions for the uranium vacancy concentrations (LANL) are implemented into phase field simulations (UF) and fuel performance simulations (INL) of sintering and FGR, respectively.

Phase field simulations of undoped, Cr-doped, and Mn-doped UO_2 sintering were carried out using MARMOT. If just the bulk vacancy concentrations were modified due to doping no effect was seen on pore closure rates (densification), indicating that grain boundary diffusion is the dominant densification mechanism. Therefore, a segregation energy was used to couple the grain boundary concentration to the bulk concentration model. Below 1803 K for Cr and 1772 K for Mn, no effect on densification was predicted because the dopants have no effect on the uranium vacancy concentration due to low solubility. Above these temperatures both Cr- and Mn-doping were shown to enhance densification compared to undoped UO_2, with Mn more effective than Cr. This is in reasonable agreement with the work of Bourgeois et al. [2], who observed a peak at 1800-1880 K in the densification rate as function of temperature for Cr-doped UO_2. However, the peak might be associated simply with the removal of a barrier to densification as solid Cr precipitates are dissolved and not necessarily with a speed up of the underlying mechanism, as predicted here. We predicted a decrease in the densification rate of undoped UO_2 as function of temperature in contradiction with experiment. This is indicative of a negative activation energy in undoped UO_2 and could be due to an over estimate of the segregation energy.

FGR simulations on Cr-doped UO_2 were carried out using BISON. The grain size in the FGR model was adjusted to 55 μm to account for enlarged grains. Additionally, the fission gas diffusivity was modified using the enhanced uranium vacancy concentrations based on atomic scale simulation results. Using the modified FGR model, BISON simulations were carried out that were representative of the Halden IFA-677.1 fuel rod experiment. The results demonstrated that the atomistically informed modification to fission gas diffusivity had no effect because fuel temperatures never reached the 1803 K threshold for enhanced diffusivity. This indicates that the reduction of FGR due to large grains is not undermined by the high temperature enhancement of fission gas diffusivity.

5. Future work

Given our current understanding, the work on developing an atomistically informed FGR model for doped UO_2 does not need further investigation. Based on the results presented here it is apparent that fission gas diffusivity is unaffected by doping for the temperatures of interest.

The fact that enhanced uranium vacancy concentrations in doped UO_2 do not undermine the beneficial effects of enlarged grains is an important result that will be disseminated in a paper as part of future work.

Further work needs to be done to improve the underlying atomic scale models and their coupling to phase field simulations of sintering, for which the understanding of grain boundaries is key. Some important areas to consider are:

1. Development of a segregation model that is dependent on the concentration of vacancies at the grain boundary, through two effects:

   (a) Site occupancy effect - Nerikar et al. [33] calculated the point uranium vacancy energy at various sites in and around a $\Sigma 5$ tilt grain boundary. This data will be used to determine the change in the segregation energy as a function of concentration due to the fact the low energy sites become fully occupied. This will be carried out using the same approach taken by Andersson et al. [34] for Xe at UO_2 grain boundaries.

   (b) Space charge effect - Due to the ionic nature of UO_2, uranium vacancies carry negative charge. As the grain boundary accumulates uranium vacancies the charge build up will repel further segregation. A modified segregation model will be developed that accounts for the effect of space change, either through an analytical description of charge density or through atomistic simulations where the lowest energy distribution of high concentrations of vacancies at grain boundaries is determined (molecular dynamics or monte-carlo simulations would be suitable). The creation of charge compensating holes at the grain boundaries might negate the effect of space charge to some extent and will also be considered.

2. Similarly to the work proposed for uranium vacancies, an understanding of the interaction of the dopant with the grain boundaries should also be developed. Firstly, an empirical potential must be derived that describes Cr or Mn in the multiple charges states predicted by DFT studies [17]. This will enable similar studies to those carried out on uranium vacancies [33] at grain boundaries to be repeated for the dopant.

3. Uberuaga and Andersson calculated the change in migration energy for a uranium vacancy at a grain boundary compared to the bulk [35]. Not only is this value expected to be dependent on the type of grain boundary but it is also varies for different directions in the grain boundary plane. It might be suitable to include different grain boundary types and orientations in the phase field simulations or just test a range of possible migration energies based on Ref. [35].

4. So far the phase field simulations have primarily addressed densification during sinter rather than grain growth. Two possible routes for enhanced grain boundary kinetics in doped UO_2 will be investigated: i) the enhancement of grain boundary uranium vacancy concentrations by doping in bulk UO_2 could make grain boundary reorientation easier, and ii) the segregation of significant concentrations of dopant to the grain boundary could

create so called grain boundary complexes [36] that can restructure the grain boundary in a way that increases their mobility. Both of these approaches are dependent first on the successful development of the segregation models described in 1 and 2.

Although outside the scope of this report, future studies will try to address the effect of dopants on fuel plasticity. For example, through the effect of impurity-dislocation and vacancy-dislocation interactions on dislocation glide or through the effect of grain size.

References

[1] M. Tonks, D. Andersson, R. Devanathan, R. Dubourg, A. El-Azab, M. Freyss, F. Iglesias, K. Kulacsy, G. Pastore, S. R. Phillpot, M. Welland, Unit mechanisms of fission gas release: Current understanding and future needs, Journal of Nuclear Materials 504 (2018) 300–317.

[2] L. Bourgeois, P. Dehaudt, C. Lemaignan, A. Hammou, Factors governing microstructure development of Cr_2O_3-doped UO_2 during sintering, Journal of Nuclear Materials 297 (2001) 313–326.

[3] V. Peres, L. Favergeon, M. Andrieu, J. C. Palussire, J. Balland, C. Delafoy, M. Pijolat, High temperature chromium volatilization from Cr_2O_3 powder and Cr_2O_3-doped UO_2 pellets in reducing atmospheres, Journal of Nuclear Materials 423 (2012) 93–101.

[4] J. C. Killeen, Fission gas release and swelling in UO_2 doped with Cr_2O_3, Journal of Nuclear Materials 88 (1980) 177–184.

[5] J. Arborelius, K. Backman, L. Hallstadius, M. Limbäck, J. Nillson, B. Rebensdorff, G. Zhou, K. Kitano, R. Löfström, G. Rönnberg, Advanced doped UO_2 pellets in LWR applications, Journal of Nuclear Science and Technology 43 (2006) 967–976.

[6] C. Riglet-Martial, P. Martin, D. Testemale, C. Sabathier-Devals, G. Carlot, P. Matheron, X. Iltis, U. Pasquet, C. Valot, C. Delafoy, R. Largenton, Thermodynamics of chromium in UO_2 fuel: A solubility model, Journal of Nuclear Materials 447 (2014) 63–72.

[7] C. Mieszczynski, G. Kuri, J. Bertsch, M. Martin, C. N. Borca, C. Delafoy, E. Simoni, Microbeam x-ray absorption spectroscopy study of chromium in large-grain uranium dioxide fuel, Journal of Physics Condensed Matter 26 (2014) 355009.

[8] H. Assmann, W. Dorr, G. Gradel, G. Maier, M. Peehs, Doping UO_2 with niobia - beneficial or not?, Journal of Nuclear Materials 98 (1981) 216–220.

[9] J. C. Killeen, The effect of additives on the irradiation behaviour of UO_2, Journal of Nuclear Materials 58 (1975) 39–46.

[10] T. Fujino, T. Shiratori, N. Sato, K. Fukuda, K. Yamada, H. Serizawa, Post-irradiation examination of high burnup Mg doped UO_2 in comparison with undoped UO_2, Mg-Nb doped UO_2 and Ti doped UO_2, Journal of Nuclear Materials 297 (2001) 176–205.

[11] P. T. Sawbridge, C. Baker, R. M. Cornell, K. W. Jones, D. Reed, J. B. Ainscough, The irradiation performance of magnesia doped UO_2, Journal of Nuclear Materials 95 (1980) 119–128.

[12] T. Fujino, S. Nakama, N. Sato, K. Yamada, K. Fukuda, H. Serizawa, T. Shiratori, Solubility of magnesium in uranium dioxide, Journal of Nuclear Materials 246 (1997) 150–157.

[13] J. B. Ainscough, F. Rigby, S. C. Osborn, The effect of titania on grain growth and densification of sintered UO_2, Journal of Nuclear Materials 52 (1974) 191–203.

[14] R. M. Leckie, E. P. Luther, Evolutionary Enhancements to UO_2, Tech. Rep. LA-UR-13-22252 (2013) M3FT-13LA020206.

[15] F. Dherbey, F. Louchet, A. Mocellin, S. Leclercq, Elevated temperature creep of polycrystalline uranium dioxide: From microscopic mechanisms to macroscopic behaviour, Acta Materialia 50 (2002) 1495–1505.

[16] M. W. D. Cooper, C. R Stanek, D. A. Andersson, Milestone Report: Calculate parameters controlling grain growth in doped UO_2 [M3MS-18LA0201035], Tech. Rep. (2018).

[17] M. W. D Cooper, C. R. Stanek, D. A. Andersson, The role of dopant charge state on defect chemistry and grain growth of doped UO_2, Acta Materialia 150 (2018) 403–413.

[18] C. R. A. Catlow, Fission gas diffusion in uranium dioxide, Proc. R. Soc. Lond. A 364 (1978) 473–497.

[19] I. Greenquist, M. Tonks, Mesoscale modeling of doped UO_2 for application as an accident tolerant fuel, NEAMS PSU Subcontract, progress report.

[20] M. Plapp, Unified derivation of phase-field models for alloy solidification from a grand-potential functional, Physical Review E 84 (2011) 1–15.

[21] L. K. Aagesen, Y. Gao, D. Schwen, K. Ahmed, Grand-potential-based phase-field model for multiple phases, grains, and chemical components, Physical Review E 98 (2018) 023309.

[22] M. R. Tonks, D. Gaston, P. C. Millett, D. Andrs, P. Talbot, An object-oriented finite element framework for multiphysics phase field simulations, Computational Materials Science 51 (2012) 20–29.

[23] M. R. Tonks, Y. Zhang, A. Butterfield, X.-M. Bai, Development of a grain boundary pinning model that considers particle size distribution using the phase field method, Modelling and Simulation in Materials Science and Engineering 23 (2015) 045009.

[24] N. Moelans, B. Blanpain, P. Wollants, Quantitative analysis of grain boundary properties in a generalized phase field model for grain growth in anisotropic systems, Physical Review B 78 (2008) 024113.

[25] J. D. Hales, R. L. Williamson, S. R. Novascone, G. Pastore, B. W. Spencer, D. S. Stafford, K. A. Gamble, D. M. Perez, R. J. Gardner, W. Liu, J. Galloway, C. Matthews, C. Unal, N. Carlson, BISON Theory Manual The Equations Behind Nuclear Fuel Analysis, Tech. rep. (2016).

[26] Y. Che, G. Pastore, J. Hales, K. Shirvan, Modeling of Cr_2O_3-doped UO_2 as a near-term accident tolerant fuel for LWRs using the BISON code, Nuclear Engineering and Design 337 (2018) 271–278.

[27] M. V. Speight, A Calculation on the Migration of Fission Gas in Material Exhibiting Precipitation and Re-solution of Gas Atoms Under Irradiation, Nuclear Science and Engineering 37 (1969) 180–185.

[28] G. Busker, A. Chroneos, R. W. Grimes, I.-w. Chen, Solution Mechanisms for Dopant Oxides in Yttria, Journal of the American Ceramics Society 82 (1999) 1553–59.

[29] M. W. D. Cooper, M. J. D. Rushton, R. W. Grimes, A many-body potential approach to modelling the thermomechanical properties of actinide oxides, Journal of Physics: Condensed Matter 26 (2014) 105401.

[30] M. W. D. Cooper, S. T. Murphy, D. A. Andersson, The defect chemistry of $UO_{2\pm x}$ from atomistic simulations, Journal of Nuclear Materials 504 (2018) 251–260.

[31] H. Matzke, Atomic transport properties in UO_2 and mixed oxides (U, Pu)O_2, Journal of the Chemical Society, Faraday Transactions 2 83 (1987) 1121–1142.

[32] J. A. Turnbull, C. A. Friskney, J. R. Findlay, F. A. Johnson, A. J. WAlter, The diffusion coefficients of gaseous and volatile species during the irradiation of uranium dioxide, Journal of Nuclear Materials 107 (1982) 168–184.

[33] P. V. Nerikar, K. Rudman, T. G. Desai, D. Byler, C. Unal, K. J. Mcclellan, S. R. Phillpot, S. B. Sinnott, P. Peralta, B. P. Uberuaga, C. R. Stanek, Grain Boundaries in Uranium Dioxide: Scanning Electron Microscopy Experiments and Atomistic Simulations, Journal of the American Ceramics Society 94 (2011) 1893–1900.

[34] D. A. Andersson, M. R. Tonks, L. Casillas, S. Vyas, P. Nerikar, B. P. Uberuaga, C. R. Stanek, Multiscale simulation of xenon diffusion and grain boundary segregation in UO_2, Journal of Nuclear Materials 462 (2015) 15–25.

[35] B. P. Uberuaga, D. A. Andersson, Uranium vacancy mobility at the $\Sigma 5$ symmetric tilt and $\Sigma 5$ twist grain boundaries in UO_2, Computational Materials Science 108 (2015) 80–87.

[36] S. J. Dillon, M. Tang, W. C. Carter, M. P. Harmer, Complexion : A new concept for kinetic engineering in materials science, Acta Materialia 55 (2007) 6208–6218.